Forward X-ray scatter from laser-shock compressed plasmas

D. Riley, F. Y. Khattak and E. Garcia-Saiz
School of Mathematics and Physics, Queen's University Belfast, University Road, Belfast, BT7 1NN, UK

G. Gregori, S. Bandyopadhyay, M. Notley and D. Neely
Central Laser Facility, CCLRC Rutherford Appleton Laboratory, Chilton, Didcot, Oxon., OX11 0QX, UK

D. Chambers, A. Moore and A. Comley
AWE plc, Aldermaston, UK

Main contact email address d.riley@qub.ac.uk

Introduction

In recent years, spectrally resolved X-ray scattering has been developed for the probing of dense plasmas[1-6]. This has been motivated by the desire to reproduce the significant success of Thomson scattering in the optical regime for lower density plasmas. So far this technique has been successful in diagnosing electron temperature in radiatively heated plasmas[1] and by comparing the contributions of strongly and weakly bound and free electrons, a technique for determining the average ionization of a sample has been developed[4]. These experiments have generally been carried out with back-scattering in the regime where the Thomson scattering parameter, α, is <1. This means that the scattering spectrum reflects short spatial scale thermal motion of the electrons rather than the longer scale collective motions that are probed when α >1. In fact, for a dense plasma, degeneracy effects mean that the definition of α has to be modified[1] and in fact attaining α > is not easy.

In a recent experiment using the VULCAN laser, we have attempted to probe in the forward direction for a laser-shock compressed sample, where we expect α~1. The experiment is shown, schematically, in figure 1. Two beams of 0.53μm laser light of ~1ns duration are focussed at 45° onto a sample foil which consists of a CH/Al/CH sandwich with thicknesses 4.5/6/4.5 microns. With phased zone plates the focal spot is 1.5mm × 2.3mm and flat topped. The beams have a sharp rise (~250ps) to 7×10^{12} Wcm^{-2} followed by a slow fall over 900ps. These are the shock driving beams for producing the "sample".

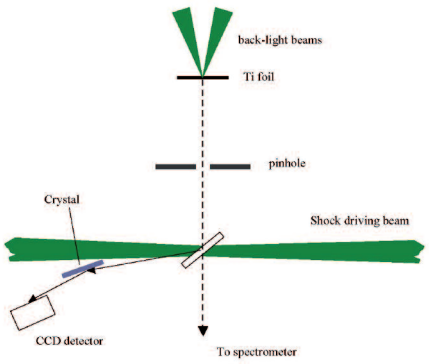

Figure 1. Schematic of experimental set-up.

Two shorter pulses (~270ps FWHM) are synchronised to the longer pulses to ~30ps accuracy. These are focussed onto a 3μm thick Ti foil at ~2×10^{15} Wcm^{-2} to create a bright source of Ti He-alpha radiation at 4.75keV. The photons from this source pass through a pinhole arrangement and fall onto the target in a cone of ~7° divergence. This cone illuminates an ellipse of 1 × 1.4mm at the foil. The X-ray beam then passes to a "back-lighter monitor" spectrometer which is a CCD fitted with a flat quartz (10-12) crystal.

The alignment of the targets and back-lighter is achieved with the use of a kinematic mounting system. Single wire and cross-wire targets are substituted for the back-light and sample foils respectively. These are used to define the positions of the real targets with respect to the target mount to an accuracy of ~10 microns. The target mount is then used with these alignment targets to focus the laser beams to the correct positions in the target chamber. Now, when the actual targets are substituted using the external alignment rig, we are sure that they are aligned such that x-rays from the back-lighter are centred on the shocked region. Taking into account the reproducibility of the laser beam alignment system we are sure that the alignment is better than 50 microns overall.

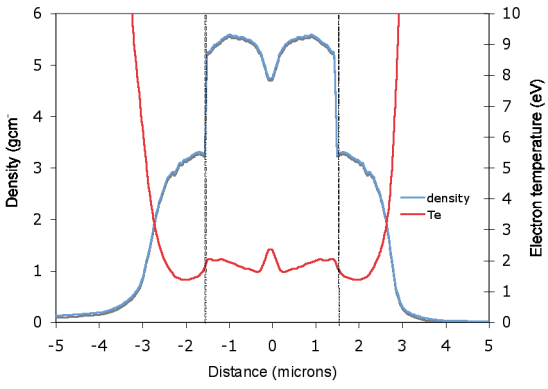

Figure 2. Simulation conditions at 0.5ns delay from the peak of the pulse, using the Hyades code. See text below for more discussion. The dashed lines mark the CH/Al boundaries.

The Ti He-alpha photons scattered at 82° are collected with a PET crystal in a von-Hamos geometry. A calibration spectrum can be taken by placing a Ti foil at the sample foil position and heating it with one of the shock driving beams with the phase plate removed. This allowed a calibration for the wavelength scale and was carried out both prior and after scatter shots and was very reproducible.

The density and temperature history of the entire foil is calculated using the HYADES code[7] including multi-group radiation transfer and the SESAME equation of state[8]. Results for one time are shown above in figure 2.

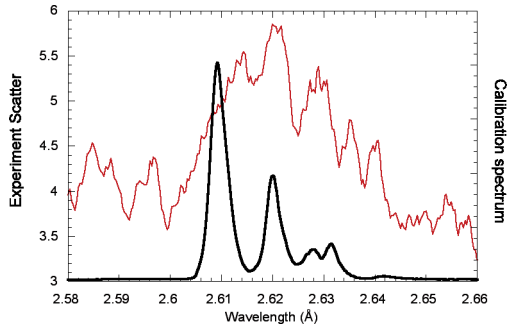

Figure 3. Typical data at a delay of 0.5ns from the peak of the pulse.

Figure 3 shows typical scatter data along with a calibration shot. We can see that the scatter data is not only broader but seems to have a peak shifted by a few mÅ from the wavelength of the principal $1s^2$-1s2p ^1P line at 2.6097Å. The input spectrum seems to be reproduced but shifted by ~10mÅ to the red as if there is a narrow but inelastic scatter mechanism.

We have simulated the data along lines similar to Gregori *et al.* [4,6] The basic terms are derived from Chihara [9] and are shown in equation 1 below:

$$S(\omega,q) = \left|f(q)+\rho(q)\right|^2 S_{ii}(q,\omega) + Z_f S_{ee}(q,\omega) + \qquad (1)$$
$$Z_B \int S_{ce}(q,\omega-\omega')S_s(q,\omega')d\omega'$$

The code takes the density and temperature of the Al and uses the TF model to derive the ionic form factor and average ionization. The free electron density and temperature are used in the RPA model to give the free electron scatter. An analytical fit to the OCP model is used to generate the static ion structure factor at the angle of scatter [10]. This fit gives a good approximation to the Galam and Hansen OCP data [11] for the very high coupling parameters found in our case. The ion-electron structure factor is found using the Boercker and More formalism [12] which is valid for high ion-ion coupling. For the bound-free contributions we take the average Z* and assume that the plasma is made up from two ionisation species, Z_{low} and $Z_{low}+1$ in proportions such that the average ionisation is Z* from the TF model. For lower ionisation states we then use the energy level data from a Hartree-fock model and the Stewart-Pyatt continuum lowering model [13] to find the binding energies of the *nl* levels. The Compton profiles from Schumacher [14] give the bound-free contribution.

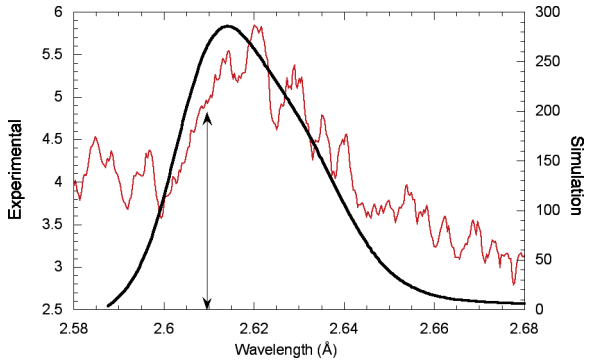

Figure 4. Simulation of scatter spectrum for the conditions in figure 2. Note that the peak shift from the resonance line position (arrow) is similar to that seen in the data and comes from the folding of the resolution into the asymmetric input spectrum. The sharper features present in the data are not present in the simulation, as expected for the large source broadening assumed.

In figure 4, we show a simulation for the case presented in figure 3. We have folded in the Ti He-alpha source spectrum and added 35eV source broadening to account for the source size presented to the spectrometer. As we can see, the general shape is reproduced. The shift in the peak is a consequence of the asymmetric nature of the incident spectrum combined with the high level of broadening. One difference between the data and simulation is that in the former, as mentioned above, there appears to be a series of narrower features that seem to be related to the resonance, inter-combination and satellite lines, but red-shifted by ~10mÅ. The origin of these features is not clear. However, if we look at short wavelength end of the spectrum in figure 3 we can see that the spectrum is quite noisy and these features may not be significant.

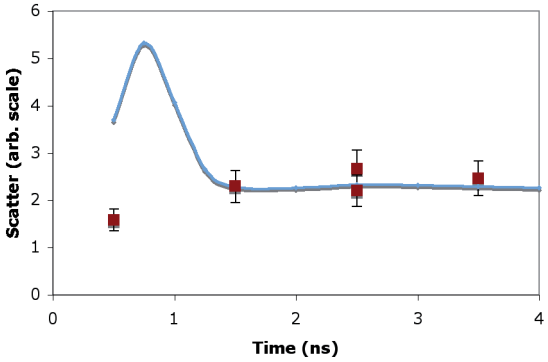

Figure 5. Simulation of scatter (solid line) against time history of total scatter from a series of shots (squares).

In figure 5 we show the time history of total scatter for a short series of shots with different delays, compared to simulation. At late time the flat behaviour is not surprising since the atoms per unit area is roughly constant and the structure factor is ~1 for lower density. Since we do not have absolute calibration we have scaled the data and simulation to agree at late time. Early in time the rapid change in coupling and hence ion-ion structure factor leads to a rapid change in total cross-section that requires better time resolution. It is possible that with a long pulse back-lighter and a streak camera instead of a CCD that this behaviour may be observed with high temporal resolution- however, the development of more sensitive streak cameras, using direct electron detection rather than phosphors may be needed before this is possible.

References

1. S. H. Glenzer, G. Gregori, R. W. Lee, F. J. Rogers, S. W. Pollaine and O. L. Landen, *Phys. Rev. Lett.* **90** 17500–1 2003
2. O. L. Landen *et al., J. Quant. Spectrosc. Radiat. Transfer* **71** pp465-478 2001
3. V. N. Tsytovich, *Astroparticle Physics* **5** pp285-298 1996
4. G. Gregori *et al., Phys. Plasmas* **11**(5) pp2754-2762 2004
5. R. Redmer, H. Reinholz, G. Ropke, R. Thiele and A. Holl, *IEEE Trans. Plasma Sci.* **33**(1) pp77-84 2005
6. G. Gregori, S. H. Glenzer, W. Rozmus, R. W. Lee and O. L. Landen, *Phys. Rev. E* **67** art. 026412 2003
7. J. T. Larsen and S. M. Lane, *J. Quant. Spectrosc. Radiat. Transfer* **51** p179 1994
8. S. P. Lyon and J. D. Johnson, LANL Group T-1. LANL report LA-UR-92-3407 1992
9. J. Chihara, *J. Phys: Condens. Matter* **12** pp231-247 2000
10. J.-L. Bretonnet and A. Derouiche, *Phys. Rev. B* **38**(13) pp9255-9256 1988
11. S. Galam and J.-P. Hansen, *Phys. Rev. A* **14**(2) pp816-832 1976
12. D. B. Boercker and R. M. More, *Phys Rev. A* **33**(3) pp1859-1869 1986
13. J. C. Stewart and K. D. Pyatt, *Astrophys. J.* **144** p1203 1966
14. M. Schumacher, F. Smend and I. Borchert, *J. Phys. B* **8** pp1428-1439 1974